# Supporting Information

## Carbon-Boron Core-Shell Microspheres for the Oxygen Reduction Reaction†

*Arun Prakash Periasamy*, [a] *Rini Ravindranath*,[a, b] *Prathik Roy*,[a] *Wen-Ping Wu*, [a] *Huan-Tsung Chang*,* [a] *Pitchaimani Veerakumar*,[c] *and Shang-Bin Liu*[c,d]

[a]*Department of Chemistry, National Taiwan University, 1, Section 4, Roosevelt Road, Taipei, 106, Taiwan*

[b]*R. Ravindranath*
*Nanoscience and Technology Program, Taiwan International Graduate Program, Academia Sinica, Taipei 11529, Taiwan.*

[c]*Institute of Atomic and Molecular Sciences, Academia Sinica, Taipei 10617, Taiwan*

[d]*National Taiwan Normal University, Taipei 11677, Taiwan*

*Prof. Huan-Tsung Chang

Department of Chemistry, National Taiwan University, 1, Section 4, Roosevelt Road, Taipei 106, Taiwan.

Tel. and fax: 011-886-2-33661171

E-mail: changht@ntu.edu.tw

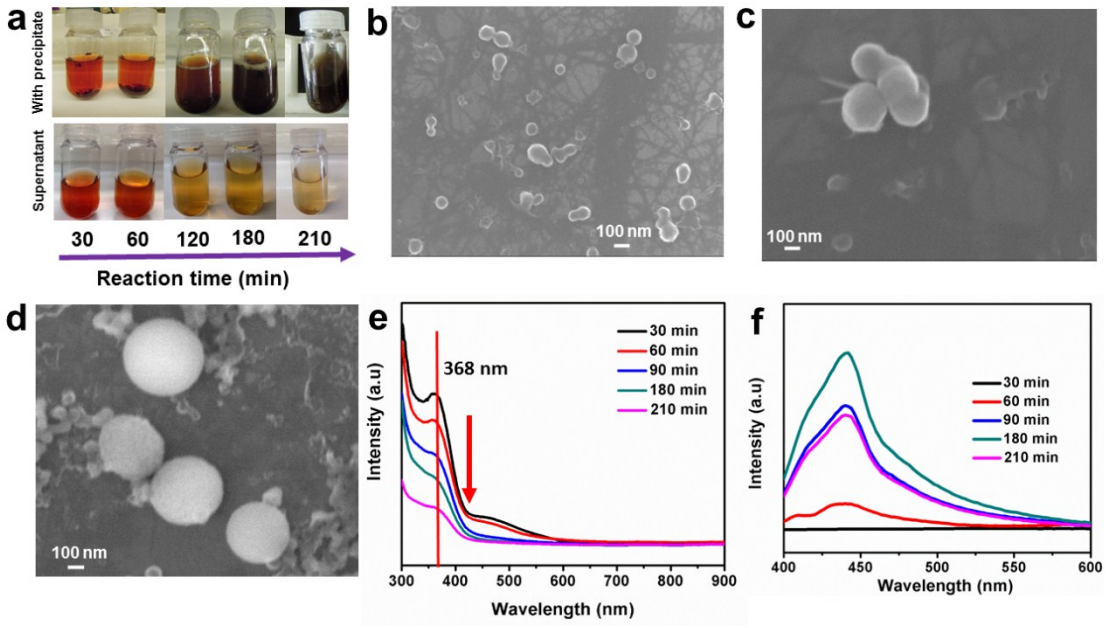


**Fig. S1** (a) Photographs of growth solutions before (top) and after centrifugation (bottom). SEM images obtained at different reaction intervals. (b) 120 (c) 180 and (d) 210 min. Time dependent UV-Vis absorption spectra (e) and fluorescence spectra (f) of the growth solutions after purification. Excitation and emission wavelengths are at 365 nm and 405 nm, respectively.

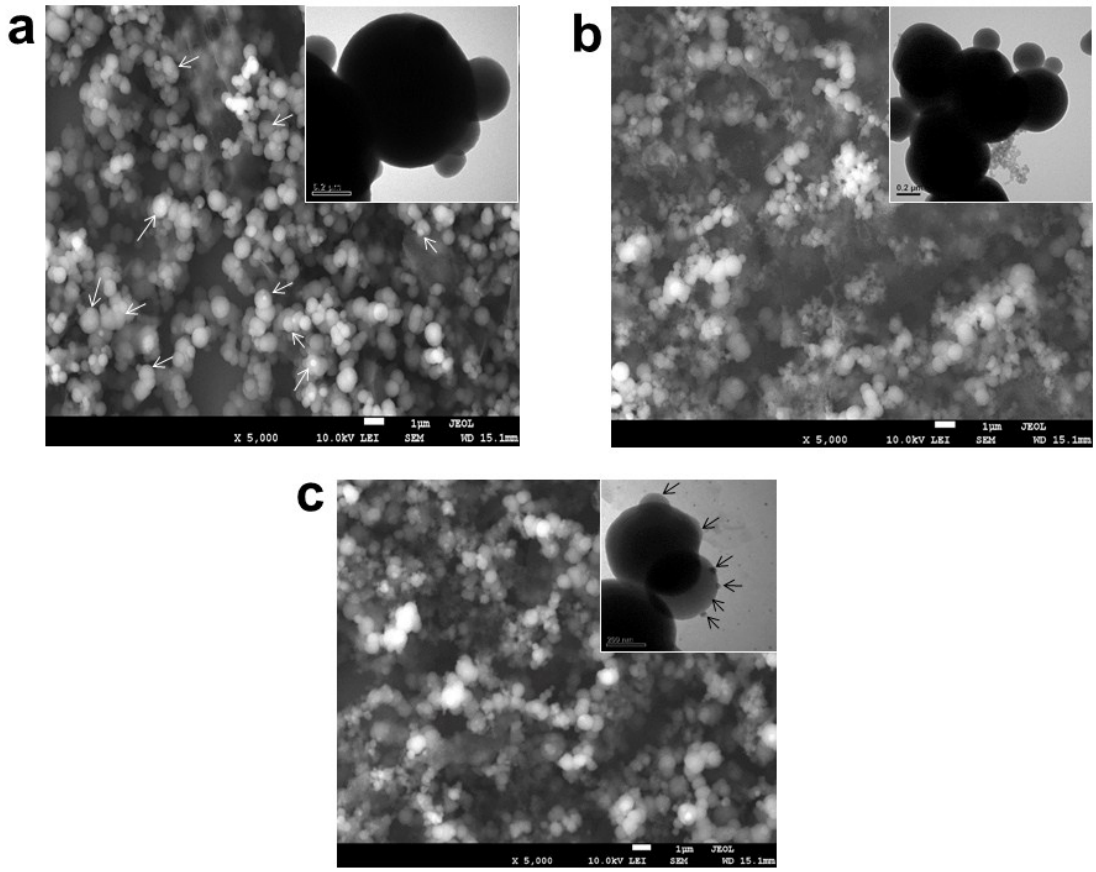


**Fig. S2** SEM images of CNM@C microspheres prepared from red onion skins at (a) 175 (b) 225 and (c) 250 $^{o}$C. Scale bars (a-c): 1 µm. Insets (a-c): magnified view of CNMs. Scale bars: 200 nm.

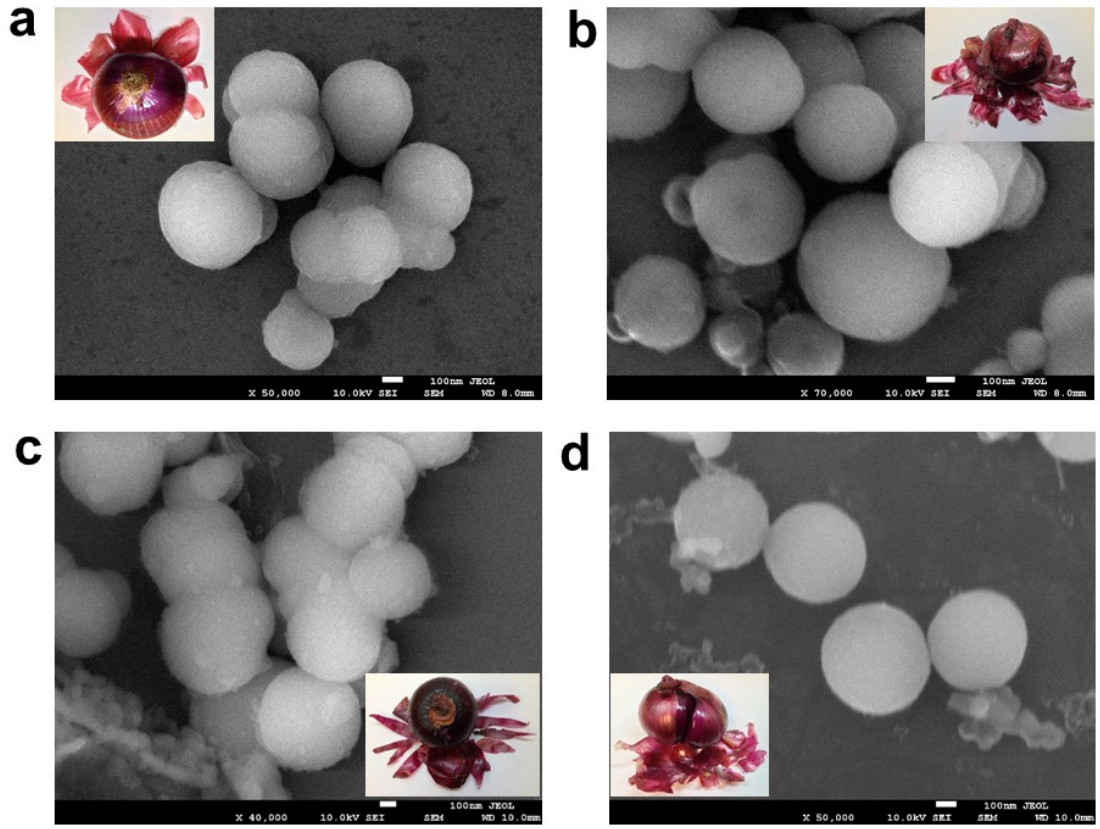


**Fig. S3** SEM images of CNM@C microspheres prepared from different red onion skins. (a) Pukekohe Long Keeper (PLK), New Zealand; radii: 5–7 cm (b) X.P. Red, Pacific RIM, single red onion; radii: 4–5 cm (c) X.P. Red, Pacific RIM, single red onion; radii: 3–4 cm (d) X.P. Red, Pacific RIM, double red onion (mutant type; radii: 4–5 cm. Insets (a-d): Photographs of each red onion with peeled skins.

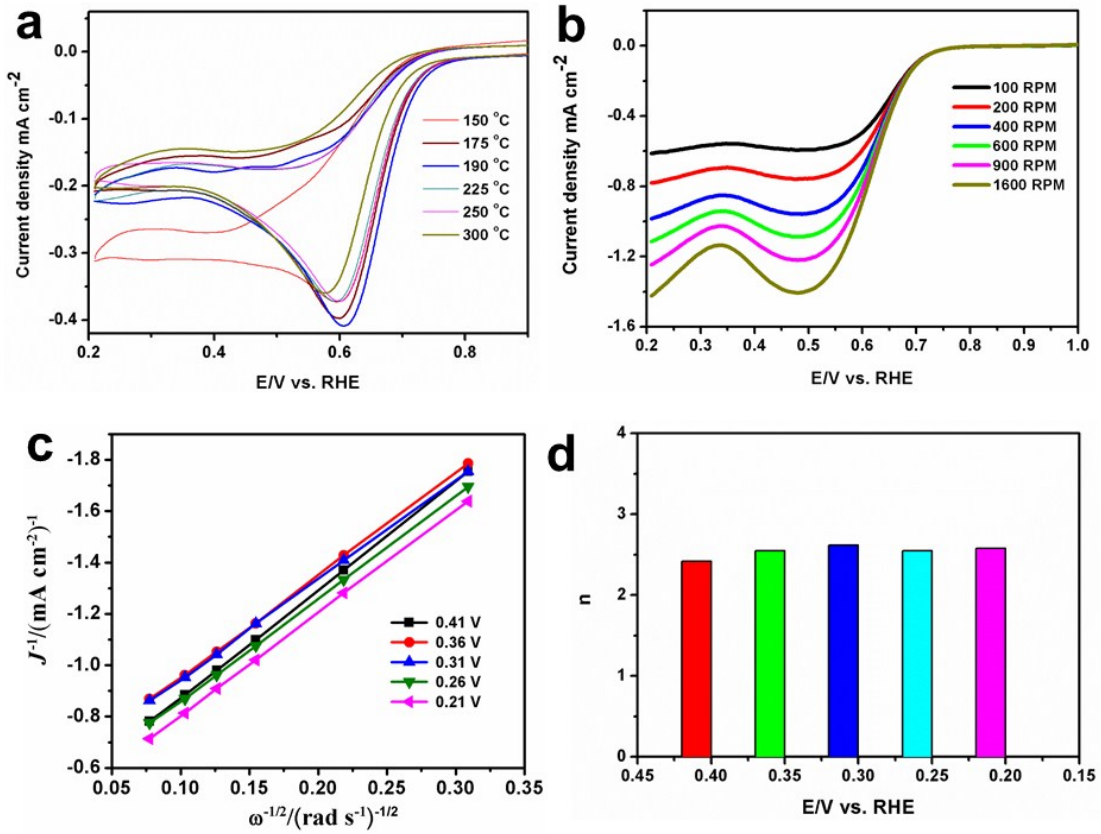


**Fig. S4** Effect of annealing temperature on the electrocatalytic activity of CNM@C microspheres for the ORR. (a) CV curves. (b) LSV polarization curves of CNM@C microspheres prepared at 190 °C at different rotation rates and at the scan rate of 5 mV $s^{-1}$. (c) Koutecky–Levich plots obtained from the data shown in (b) at different potentials. (d) Electron transfer number determined from the data provided in (c).

The kinetics of the ORR occurring at the CNM@C microsphere electrode is determined using Koutecky-Levich equations (2-4):[1, 2]

$$\frac{1}{J} = \frac{1}{J_L} + \frac{1}{J_K} \tag{2}$$

$$J_L = 0.62nFC_0D_O^{\frac{2}{3}}\upsilon^{-\frac{1}{6}}\omega^{\frac{1}{2}} \tag{3}$$

$$J_K = nFKC_O \tag{4}$$

The values of current density ($J$), limiting current density ($J_L$), kinetic current density ($J_k$), rotation rate ($\omega$ = rad $s^{-1}$), Faraday constant (F = 96485.34 C $mole^{-1}$), saturated oxygen concentration ($C_o$ ~1.14 x $10^{-5}$ mol $cm^3$), diffusion coefficient of oxygen ($D_0$ ~1.73 × $10^{-5}$ $cm^2$ $s^{-1}$) and kinetic viscosity of the solution ($v$ = 0.01 $cm^2$ $s^{-1}$) were brought to equations (2) to (4) to calculate the electron transfer rate constant ($k$) value to be 7.7 x $10^{-3}$ cm $s^{-1}$.

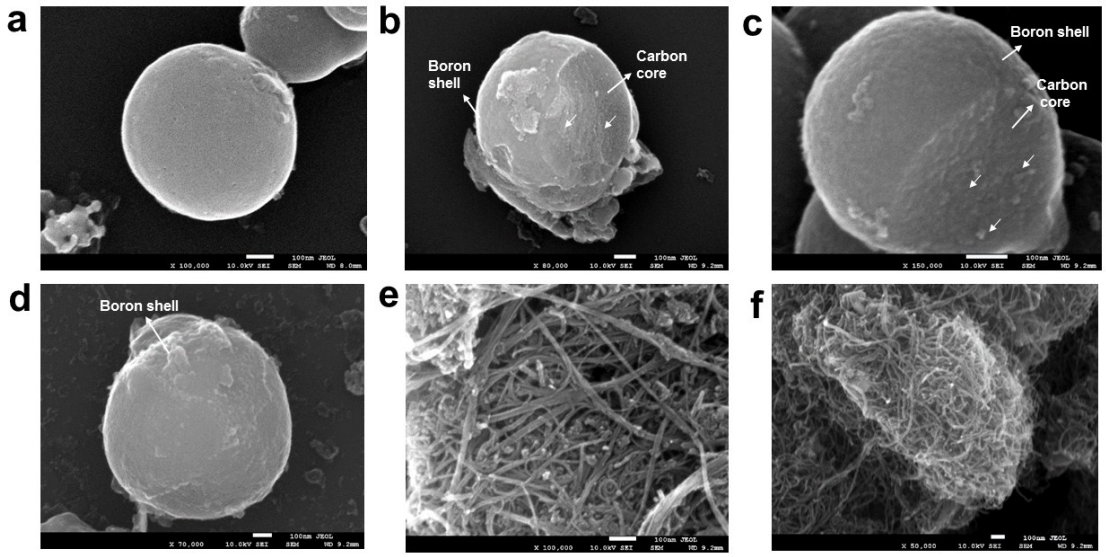


**Fig. S5** SEM images of (a) CNM@C microspheres, (b) $B_{0.1}$CNM@$C_{1.0}$ microspheres, (c) $B_{0.25}$CNM@$C_{1.0}$ microspheres, (d) $B_{1.0}$CNM@$C_{1.0}$ microspheres and (e) $B_{0.5}$SWCNT$_{1.0,}$ and (f) $B_{0.5}$MWCNT$_{1.0}$. Scale bars: 100 nm.

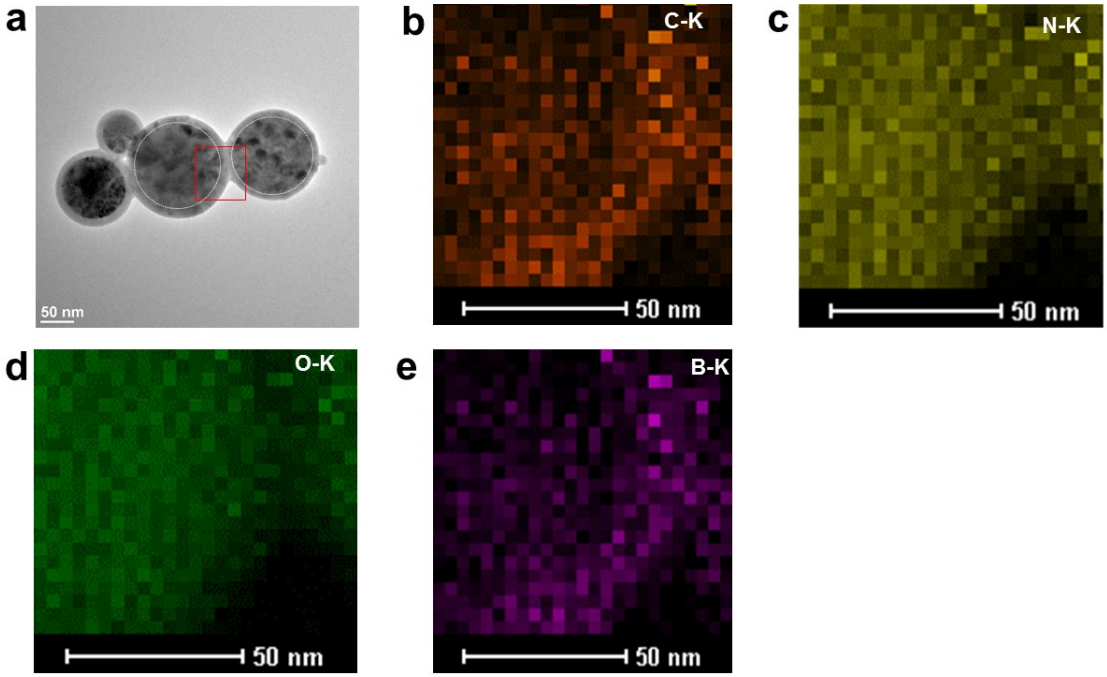


**Fig. S6.** (a) High resolution STEM image of $B_{0.5}CNM@C_{1.0}$ microspheres and mapping of elements (b) C-K, (c) N-K, (d) O-K and (e) B-K in the marked area in (a).

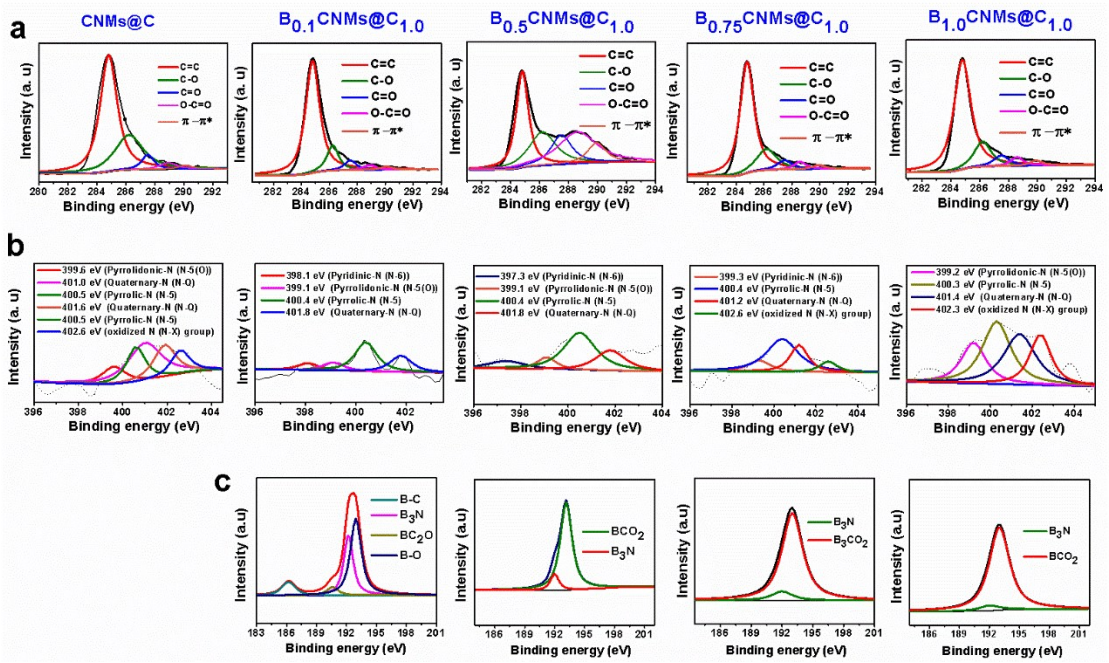


**Fig S7.** Deconvoluted (a) C1s (b) N1s and (c) B1s core level spectra of pristine CNM@C and $B_x$CNM@$C_y$ microspheres.

The C1s core level spectrum of pristine CNM@C sample displays a characteristic peak at 284.8 eV, which is deconvoluted into four peaks (Fig. S7a). The peak at 286.15 eV is assigned to the epoxide group (C-O-C) and that at 287.5 and 288.9 eV are attributed to that for carbonyl (C=O) and carboxyl groups (COOH), respectively.[3] Relative to pristine CNM@C microspheres, $B_x$CNM@$C_y$ microspheres displays a characteristic peak at 284.6 eV without any shifts in the binding energies. All these characteristic peaks (C-O-C, C=O and C-OOH) were also found at the same binding energies without any shifts, revealing boric acid treatment did not cause any change to the carbon atoms present in the graphitic planes. Fig. S7b displays the N1s core level spectra of pristine CNM@C microspheres. The characteristic peak at 400.5 is attributed to the pyrrolic-N, while that at 397.4, 399.1 and 401.7 are attributed to that for pyridinic-N, pyrrolidonic-N and quarternary-N, respectively.[4] The intensity

for the pyrrolic-N peak of $B_{0.1}$CNM@$C_{1.0}$ microspheres is higher than that of pristine CNM@C microspheres, which attributes to that for efficient binding of N atoms with the carbon atoms in the five membered rings and that at the edges of graphene.[5] The intensity for pyrrolic-N and quaternary-N peaks increased upon increasing C/B ratio, revealing binding of N atoms with the C atoms at the edges and in the bulk. Deconvoluted B1s core level spectrum of $B_{0.1}$CNM@$C_{1.0}$ sample shows four characteristic peaks at the binding energies of 186.2, 190.6, 192.1, 193 eV, which are attributed to that for B-C, $BC_2O$, $B_3N$ and B-O species, respectively (Fig. S7c).[6, 7] The products prepared at different C/B mass ratios also exhibit the characteristic peaks at 192.0 and 193 eV without any shifts, revealing the presence of $B_3N$ and B-O bonds, respectively.

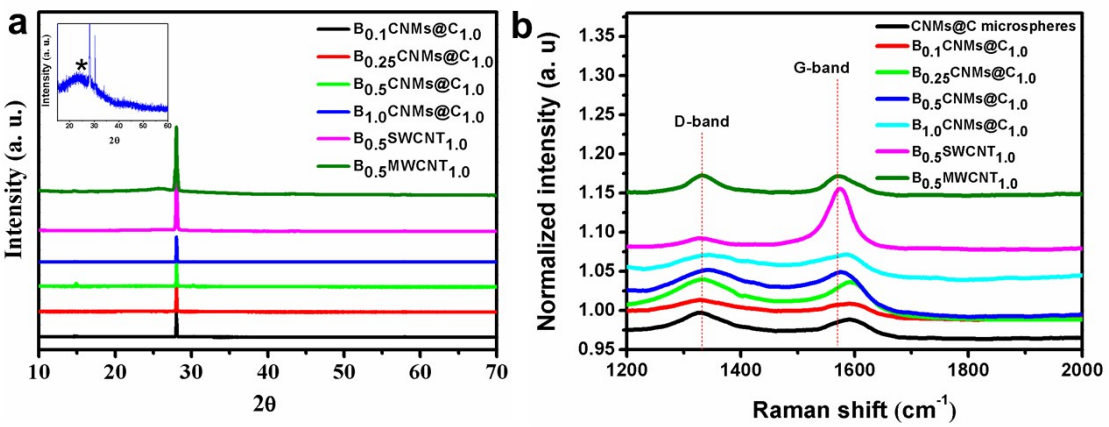


**Fig. S8.** (a) XRD and (b) Raman spectra of CNM@C microspheres with different C/B mass ratios. Controls: CNM@C microspheres, $B_{0.5}SWCNT_{1.0,}$ and $B_{0.5}MWCNT_{1.0}$ samples prepared at the optimal C/B mass ratio (1:0.5). Inset to (a): Magnified view of XRD spectrum of $B_{1.0}CNM@C_{1.0}$ reveals a broad peak (*) at around $2\Theta = 26^{O}$.

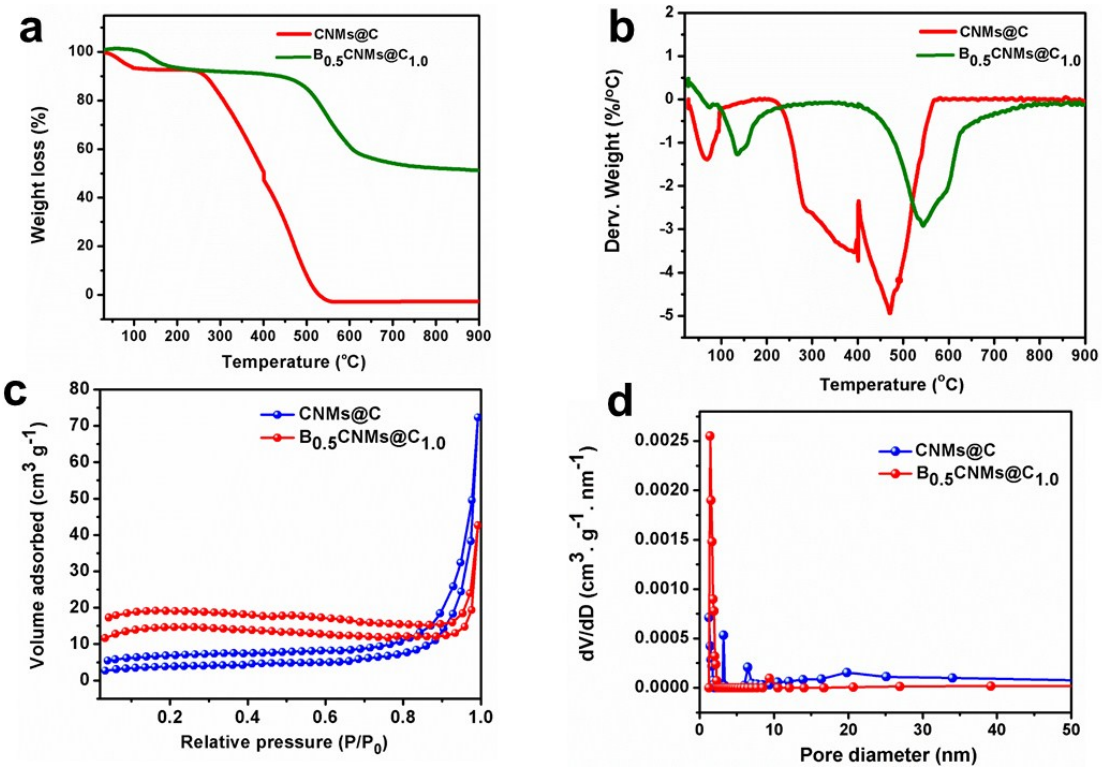


**Fig. S9.** (a) TGA (b) DTA and (c) $N_2$ adsorption-desorption curves, and (d) BJH pore size distribution of CNM@C and $B_{0.5}$CNM@$C_{1.0}$ microspheres.

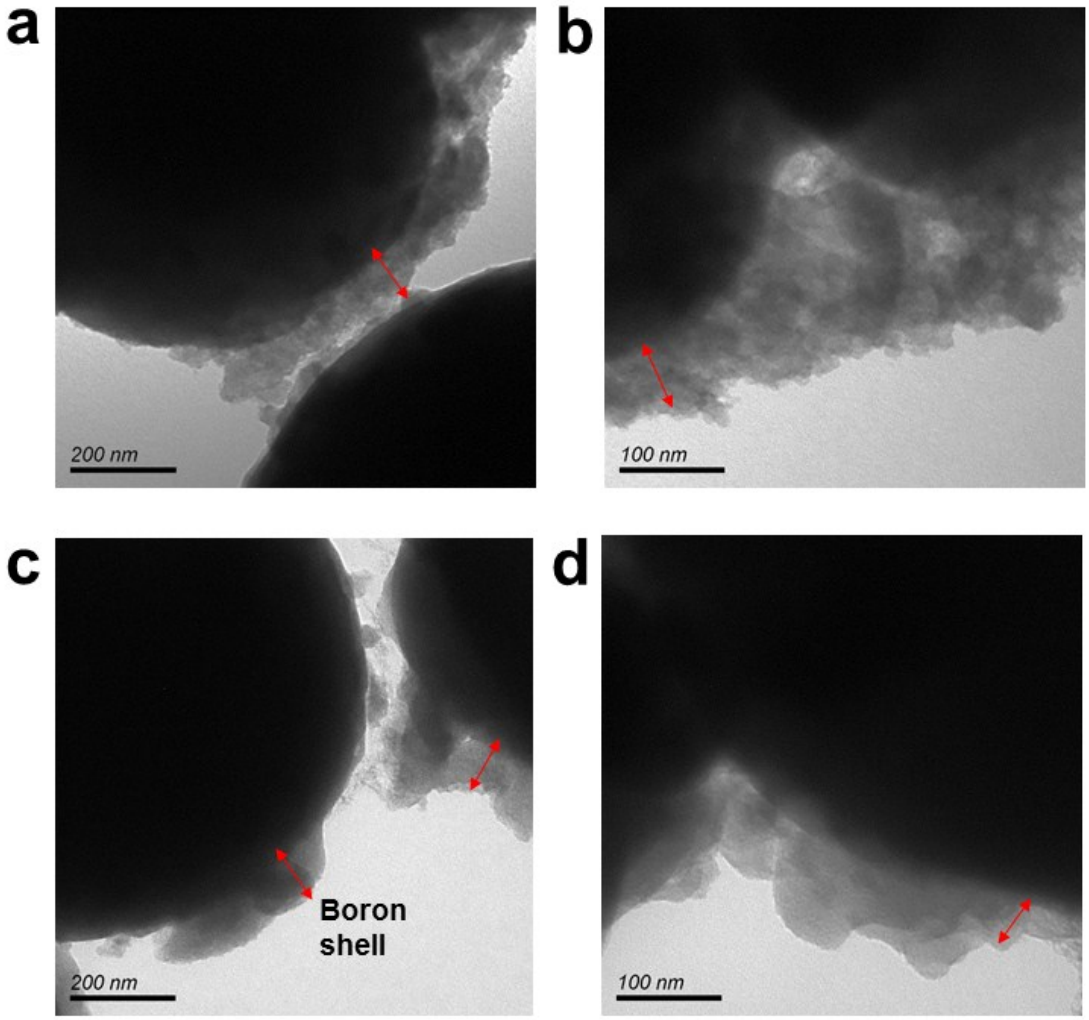


**Fig. S10.** TEM images of $B_{0.5}CNM@C_{1.0}$ samples before (a-b) and after (c-d) annealed in air at 900 °C.

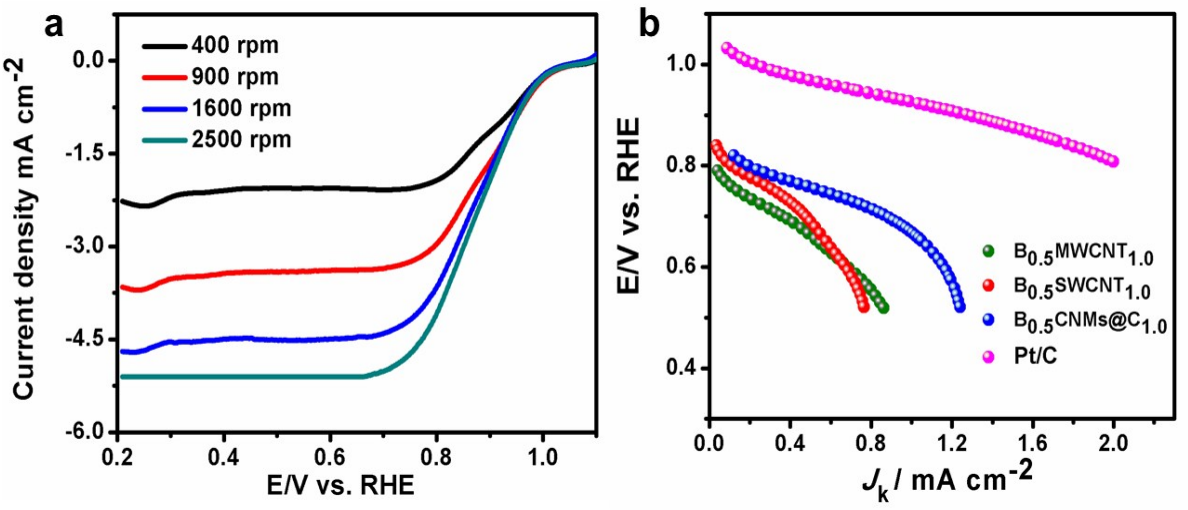


**Fig. S11.** LSV polarization curves of Pt/C RDE at different rotation rates and at the scan rate of 5 mV $s^{-1}$ (a) and mass transport corrected Tafel plots of different electrocatalysts (b).

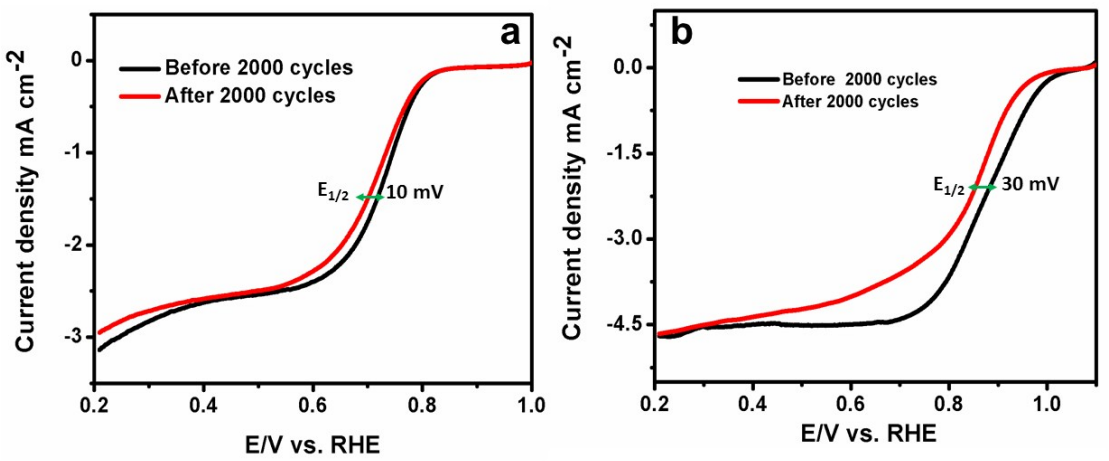


**Fig. S12** LSV polarization curves of $B_{0.5}CNM@C_{1.0}$ (a) and Pt/C (b) electrodes recorded before and after 2000 cycles of accelerated durability tests. Scan rate: 5 mV $s^{-1}$.

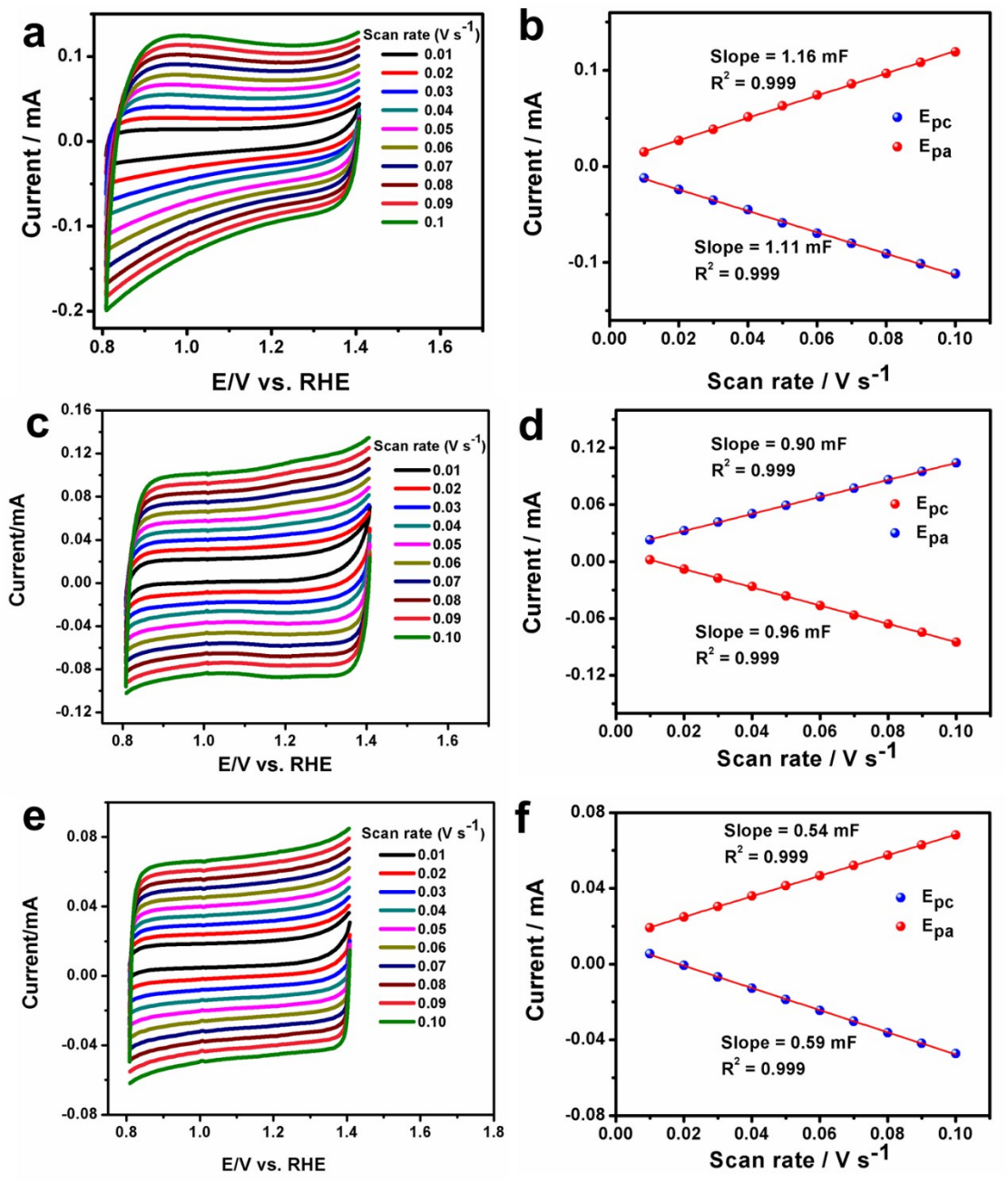


**Fig. S13** CV curves of $B_{0.5}CNM@C_{1.0}$ (a) $B_{0.5}SWCNT_{1.0}$ (c), and $B_{0.5}MWCNT_{1.0}$ (e) electrodes in 0.1 M KOH at different scan rates. Plots of double layer capacitance vs. scan rate (b-f). The double layer capacitance values were calculated from the average of the slope values.

Table S1 Elemental composition of electrocatalysts determined by elemental analysis and XPS analysis.

| Samples | Carbon | Oxygen | Hydrogen | Nitrogen | Boron |
|---|---|---|---|---|---|
| CNM@C | 44.2 | 43.0 | 5.7 | [a]2.2 | - |
| $B_{0.5}$CNM@$C_{1.0}$ | 29.7 | 22.2 | 2.8 | [b]1.7 | [c]16.2 |

[a-c]Nitrogen and Boron contents were determined using XPS analysis.

Table S2 Comparison of the ORR performance of different heteroatom doped catalysts

| Nanomaterials | LSV Onset (V) | CV Peak potential (V) | $E_{1/2}$ (V) | Stability (%) /Time (h) | Ref. |
|---|---|---|---|---|---|
| CNT/HDC-1000 | 0.92 | [a]NA | 0.82 | 95.5/1000 cycles | [8] |
| N, P-CNTs | 0.95 | 0.67 | 0.79 | 95.8/3 | [9] |
| B-N Graphene | 1.02 | 0.67 | 0.70 | >90/80 | [10] |
| $B_{20}$-MWCNTs$_{1.0}$ | 0.81 | 0.66 | 0.74 | NA | [11] |
| $B_3$CNTs | 0.74 | 0.61 | NA | NA | [12] |
| BCNMs | 0.78 | 0.61 | 0.74 | 90/11 | [13] |
| N-doped C-dots | 0.81 | 0.61 | 0.58 | 91/1.9 | [14] |
| BCN graphene | 0.83 | 0.73 | 0.76 | 90/11.1 | [15] |
| CNM@C | 0.72 | 0.6 | 0.62 | - | This work |
| $B_{0.1}$CNM@$C_{1.0}$ | 0.76 | 0.62 | 0.65 | - | This work |
| $B_{0.25}$CNM@$C_{1.0}$ | 0.76 | 0.70 | 0.70 | - | This work |
| $B_{0.5}$CNM @$C_{1.0}$ | 0.79 | 0.72 | 0.72 | 80.7/4.4 | This work |
| $B_{0.75}$CNM @$C_{1.0}$ | 0.76 | 0.71 | 0.70 | - | This work |
| $B_{1.0}$CNM @$C_{1.0}$ | 0.78 | 0.71 | 0.68 | - | This work |
| Pt/C | 0.98 | 0.67 | 0.88 | 73/4.4 | This work |

[a]not available; all potentials were converted to RHE scale.

## References


1. A. J. Bard and L. R. Faulkner, *Electrochemical methods: fundamentals and applications*, Wiley New York, 1980.
2. A. P. Periasamy, W.-P. Wu, G.-L. Lin, Z.-Y. Shih, Z. Yang and H.-T. Chang, *J. Mater. Chem A*, 2014, **2**, 11899-11904.
3. A. Ganguly, S. Sharma, P. Papakonstantinou and J. Hamilton, *J. Phys. Chem. C.*, 2011, **115**, 17009-17019.
4. F. Braghiroli, V. Fierro, M. Izquierdo, J. Parmentier, A. Pizzi and A. Celzard, *Carbon*, 2012, **50**, 5411-5420.
5. L. Lai, J. R. Potts, D. Zhan, L. Wang, C. K. Poh, C. Tang, H. Gong, Z. Shen, J. Lin and R. S. Ruoff, *Energy Environ. Sci.*, 2012, **5**, 7936-7942.
6. J.-i. Ozaki, N. Kimura, T. Anahara and A. Oya, *Carbon*, 2007, **45**, 1847-1853.
7. S. Baik and J. W. Lee, *RSC Adv.*, 2015, **5**, 24661-24669.
8. Y. J. Sa, C. Park, H. Y. Jeong, S. H. Park, Z. Lee, K. T. Kim, G. G. Park and S. H. Joo, *Angew. Chem.*, 2014, **126**, 4186-4190.
9. J. Zhu, S. P. Jiang, R. Wang, K. Shi and P. K. Shen, *J. Mater. Chem A*, 2014, **2**, 15448-15453.
10. Y. Zheng, Y. Jiao, L. Ge, M. Jaroniec and S. Z. Qiao, *Angew. Chem.*, 2013, **125**, 3192-3198.
11. Y. Cheng, Y. Tian, X. Fan, J. Liu and C. Yan, *Electrochim. Acta*, 2014, **143**, 291-296.
12. L. Yang, S. Jiang, Y. Zhao, L. Zhu, S. Chen, X. Wang, Q. Wu, J. Ma, Y. Ma and Z. Hu, *Angew. Chem.*, 2011, **123**, 7270-7273.

13. G. Panomsuwan, N. Saito and T. Ishizaki, *Electrochem. Commun.*, 2015, **59**, 81-85.

14. C. Zhu, J. Zhai and S. Dong, *Chem. Commun.*, 2012, **48**, 9367-9369.

15. S. Wang, L. Zhang, Z. Xia, A. Roy, D. W. Chang, J. B. Baek and L. Dai, *Angew. Chem. Int. Ed.*, 2012, **51**, 4209-4212.